Adhesion and hemifusion of cytoplasmic myelin lipid membranes are highly dependent on the lipid composition

ARTICLE *in* BIOCHIMICA ET BIOPHYSICA ACTA · OCTOBER 2011

Impact Factor: 4.66 · DOI: 10.1016/j.bbamem.2011.10.015 · Source: PubMed

4 AUTHORS, INCLUDING:

Xavier Banquy
Université de Montréal
61 PUBLICATIONS **612** CITATIONS
SEE PROFILE

Dong Woog Lee
University of California, Santa Barbara
38 PUBLICATIONS **323** CITATIONS
SEE PROFILE

Jacob Israelachvili
University of California, Santa Barbara
282 PUBLICATIONS **19,590** CITATIONS
SEE PROFILE

Biochimica et Biophysica Acta 1818 (2012) 402–410

Contents lists available at SciVerse ScienceDirect

Biochimica et Biophysica Acta

journal homepage: www.elsevier.com/locate/bbamem

Adhesion and hemifusion of cytoplasmic myelin lipid membranes are highly dependent on the lipid composition ☆

Xavier Banquy [a,1], Kai Kristiansen [a,1], Dong Woog Lee [a,1], Jacob N. Israelachvili [a,b,*]

[a] Department of Chemical Engineering, University of California at Santa Barbara, CA 93106, USA
[b] Materials Department, University of California at Santa Barbara, CA 93106, USA

ARTICLE INFO

Article history:
Received 15 July 2011
Received in revised form 14 October 2011
Accepted 18 October 2011
Available online 25 October 2011

Keywords:
Multiple sclerosis
Hemi-fusion
Lipid membrane

ABSTRACT

We report the effects of calcium ions on the adhesion and hemifusion mechanisms of model supported myelin lipid bilayer membranes of differing lipid composition. As in our previous studies Min et al. [1,2], the lipid compositions used mimic "healthy" and "diseased-like" (experimental autoimmune encephalomyelitis, EAE) membranes. Our results show that the interaction forces as a function of membrane separation distance are well described by a generic model that also (and in particular) includes the hydrophobic interaction arising from the hydrophobically exposed (interior) parts of the bilayers. The model is able to capture the mechanical instability that triggers the onset of the hemifusion event, and highlights the primary role of the hydrophobic interaction in membrane fusion. The effects of lipid composition on the fusion mechanism, and the adhesion forces between myelin lipid bilayers, can be summarized as follows: in calcium-free buffer, healthy membranes do not present any signs of adhesion or hemifusion, while diseased membranes hemifuse easily. Addition of 2 mM calcium favors adhesion and hemifusion of the membranes independently of their composition, but the mechanisms involved in the two processes were different: healthy bilayers systematically presented stronger adhesion forces and lower energy barriers to fusion compared to diseased bilayers. These results are of particular relevance for understanding lesion development (demyelination, swelling, vacuolization and/or vesiculation) in myelin associated diseases such as multiple sclerosis and its relationship to lipid domain formation in myelin membranes.

Published by Elsevier B.V.

1. Introduction

The myelin membrane sheath plays a key role for efficient and precise operation of nerve cells in the central nervous system (CNS) [3] by acting as an electrical insulator. The membrane is wrapped around the axon of nerve cells in multiple layers extending up to a few tens of micrometers in diameter. The structure of these multiple layers alternates in a radial direction between cytoplasmic and extracellular faces separated by 3–4 nm thick aqueous layers [4], and these faces have very different lipid and protein compositions. Under physiological conditions, the myelin sheath shows strong adhesion between the lipid layers [2]. Any small alteration of the composition and interaction *within* the layers and/or *between* these layers can cause swelling across the water gaps, vacuolization, vesiculation, or even disintegration of the myelin structure and, as a consequence, deterioration of nerve cell function. This demyelination of axons is believed to be a sign of autoimmune diseases like EAE or Multiple Sclerosis (MS) [5].

A characteristic feature of the myelin membrane is the unusually high concentration of lipids [6] compared to other mammalian cells. Moreover, the lipid and protein distribution across these myelin bilayers is significantly asymmetric. The Myelin Basic Protein (MBP) is the second most abundant protein in the myelin sheath and is found only at the cytoplasmic interface. Recent studies have shown that MBP provides additional adhesion between lipid layers through a combination of hydrophobic and electrostatic interactions [2,7–10], but the lipid bilayers alone also show adhesive properties [10]. The adhesive properties of lipid bilayers point out that the interaction energy between the myelin lipid bilayers themselves may play an

Abbreviations: a, molecular area of the lipid molecules; a_0, unperturbed molecular area of the lipid molecules; A, surfaces contact area; A_{hem}, hemifused area; C_{ES}, C_{HI}, C_{SI}, constant pre-factor; D_{ES}, D_{HI}, D_{SI}, characteristic decay length; D_w, water gap thickness; D_b, bilayer thickness; D_{ad}, separation distance at which jump out occurs; D, separation distance; E, total molecular energy of the lipids in the bilayers; e, is the electronic charge; F, total interaction force; F_{ad}, adhesion force between bilayers; F_c, critical force at which breakthrough occurs; k, is the Boltzmann constant; R, radius of the surfaces; r, radius of the contact area; T, temperature; W, total interaction energy; z, ion valency; γ_i, interfacial tension of the hydrocarbon–water interface; ψ, the surface potential of the membrane; σ, effective surface charge density

☆ XB, KK, DWL and JNI designed research; XB, DWL and KK performed research; XB and KK analyzed data; XB, KK, DWL and JNI wrote the paper.

* Corresponding author at: Department of Chemical Engineering, University of California (M/C 5080) Santa Barbara, CA 93106-5080, USA. Tel.: +1 805 893 8407; fax: +1 805 893 7870.
E-mail address: Jacob@engineering.ucsb.edu (J.N. Israelachvili).

[1] XB, KK and DWL contributed equally to this work.

0005-2736/$ – see front matter. Published by Elsevier B.V.
doi:10.1016/j.bbamem.2011.10.015

important role for both the structure and interactions of myelin membranes.

The interaction forces between the lipid bilayers are dependent on several factors including the charges on the lipid head groups and the degree of unsaturation of the lipid hydrocarbon chain. We believe that changes in the lipid membrane composition are one of the main factors leading to defective development of the myelin sheaths [11–13].

In this work we have focused on the myelin lipid bilayer–bilayer interaction, and have changed the lipid composition in order to mimic healthy and diseased myelin membranes. We paid particular attention to the contribution of the cytoplasmic layer lipid composition. By comparing the interaction forces found in healthy and diseased bilayers we are seeking to identify the physical properties that cause demyelination. The supported model bilayers with different cytoplasmic layer compositions (see Table 1) were constructed. The adhesion forces were measured using a Surface Forces Apparatus (SFA) 2000 [14]. This method [15] suppresses certain membrane-membrane interaction like the undulation force [10], but emphasizes the other forces such as the electrostatic, steric hydration, van der Waals and hydrophobic forces.

2. Materials and methods

2.1. Materials

Our previous work [10] identified differences in lipid compositions in healthy and diseased marmosets white matter using nuclear magnetic resonance (NMR) and high performance liquid chromatography (HPLC) techniques. Table 1 shows the cytoplasmic lipid compositions of healthy (control) and experimental allergic encephalomyelitis (EAE, diseased) white matter. In this work, the following porcine brain-derived lipids were used to mimic the cytoplasmic leaflet of myelin membrane: phosphatidylserine (Porcine brain PS−), sphingomyelin (Porcine brain SM), phosphatidylcholine (Porcine brain PC), phosphatidylethanolamine (Porcine brain PE), and cholesterol (ovine wool) (Avanti Polar Lipids, Alabaster, AL, purity >99%). The major fatty acid chain lengths of the three major lipids (PC, PE and PS−) are 16:0, 18:0, 18:1 and 20:4. All lipids were stored in chloroform until used. Lipids were used as received without any further characterization. Plasmalogen content of the different lipids is unknown. Lipids used to prepare healthy and diseased bilayers were from the same batch. Dipalmitoylphosphatidylethanolamine (DPPE), sodium nitrate (purity ≥99.0%), morpholine-propanesulfonic acid (Mops) sodium salt (purity ≥99.5%), and calcium nitrate (purity ≥99.0%) were purchased from Sigma-Aldrich (St. Louis, MO). The following solvents were used to disperse lipids: hexane (RegentPlus®, purity ≥99.0%), chloroform (CHROMASOLVE® Plus, for HPLC, purity ≥99.9%), ethanol (200 proof, HPLC/spectrophotometric grade), and methanol (CHROMASOLVE® Plus, for HPLC, purity ≥99.9%) (Sigma-Aldrich, St. Louis, MO).

Table 1
Lipid compositions used for the inner (cytoplasmic) myelin monolayers [1][a].

Lipid	Lipid + cholesterol composition (mole%)[b]		Lipid composition (mole%)[c]	
	Healthy (control)	Diseased (EAE)	Healthy (control)	Diseased (EAE)
Cholesterol (CHOL)	31.6	37.4	–	–
Phosphatidylserine (PS −)	7.3	7.4	10.6	11.9
Sphingomyelin (SM +/−)	6.2	2.2	9.1	3.5
Phosphatidylcholine (PC +/−)	25.9	20.1	37.9	32.1
Phosphatidylethanolamine (PE +/−)	29.0	32.9	42.4	52.5

[a] Phosphatidylinositol was not detected in ref. [10] and therefore was intentionally omitted in this study.
[b] Composition of the bilayer used in this study. The PS concentration in the EAE monolayer was adjusted to give a similar overall (inner and outer layers) charge density to EAE and control monolayers as already reported in [1].
[c] Since cholesterol molecular area is negligible in the bilayers, the composition of the bilayers was recalculated excluding cholesterol in order to emphasize on the species that really contribute to the lipid membrane superficial properties.

2.2. Substrate preparation

Atomically smooth mica surfaces were freshly cleaved under a laminar flow hood and immediately deposited on another large freshly cleaved mica backing sheet for storage. In this way, the mica interface in adhesive contact with the backing sheet is kept free from dust contamination while the other interface can be coated with silver. The thickness of the mica sheets was 2.5–3.5 μm. The thickness of the silver coating was kept constant (55 nm) and deposited by Joule effect vapor deposition. Before deposition of lipid bilayers, the silvered mica sheets were glued, silvered side down, on silica cylindrical disks using a hard epoxy glue (EPON 1004 F® from Exxon Chemicals) [16–18].

2.3. Preparation of mica supported bilayers

Fully developed lipid bilayers were deposited on the back silvered mica sheets using the Langmuir–Blodgett (LB) deposition technique [19]. For the first monolayer, 100 μl of 1 mg/ml DPPE solution (3:1 (v/v) chloroform/methanol) was deposited at a surface pressure of 35 mN/m (molecular area of ~43 Å^2) with a subphase of milliQ® water. At this surface pressure, the DPPE monolayer is in the solid state and forms a stable and atomically smooth hydrophobic monolayer on mica. After deposition, the substrates were placed in a desiccator and allowed to rest under low pressure for 12 h [20]. For the second monolayer, healthy (control) myelin and diseased (EAE) lipid solutions were prepared at the compositions summarized in Table 1 in an 11:5:4 (v/v) hexane/chloroform/ethanol solution. The second monolayer deposition was performed on the previously deposited DPPE monolayer at a surface pressure of 30 mN/m (molecular area of ~50–52 Å^2) with a subphase of sodium nitrate buffer (150 mM sodium nitrate/10 mM Mops sodium salt, pH 7.4), followed by transfer into the SFA chamber, previously filled with degassed saturated lipid solution (sodium nitrate buffer in contact with lipid crystals for 12 h prior to experiment).

2.4. Measuring interaction forces and visualizing the surfaces using the Surface Forces Apparatus (SFA)

The Surface Force Apparatus model 2000 (SFA 2000) [14] was used in this study for accurate force–distance measurements. Fig. 1 shows schematically the experimental configuration of the two interacting surfaces with their supported bilayers in the SFA. The two myelin membranes with either healthy or diseased cytoplasmic lipid composition were prepared in the LB trough as described above and transferred into the SFA box in small beakers in order to keep the bilayers constantly immersed in the aqueous solution [19,21]. The upper surface was installed on a fixed solid mount while the lower surface was supported by a double cantilever (force-measuring) spring. A motorized mechanism connected to the lower surface allows for moving the two surfaces relative to each other at controlled speed or displacement step.

The separation distance between the two surfaces is measured using optical interferometry [16]: a white light beam is shined through the surfaces and the interference fringes generated from the reflections of the light beam between the two silvered mica sheets are analyzed in a spectrometer equipped with a digital camera (Hamamatsu Orca 03G, USA). The separation distance D between the surfaces is calculated (to ±1 Å) from the wavelength of the

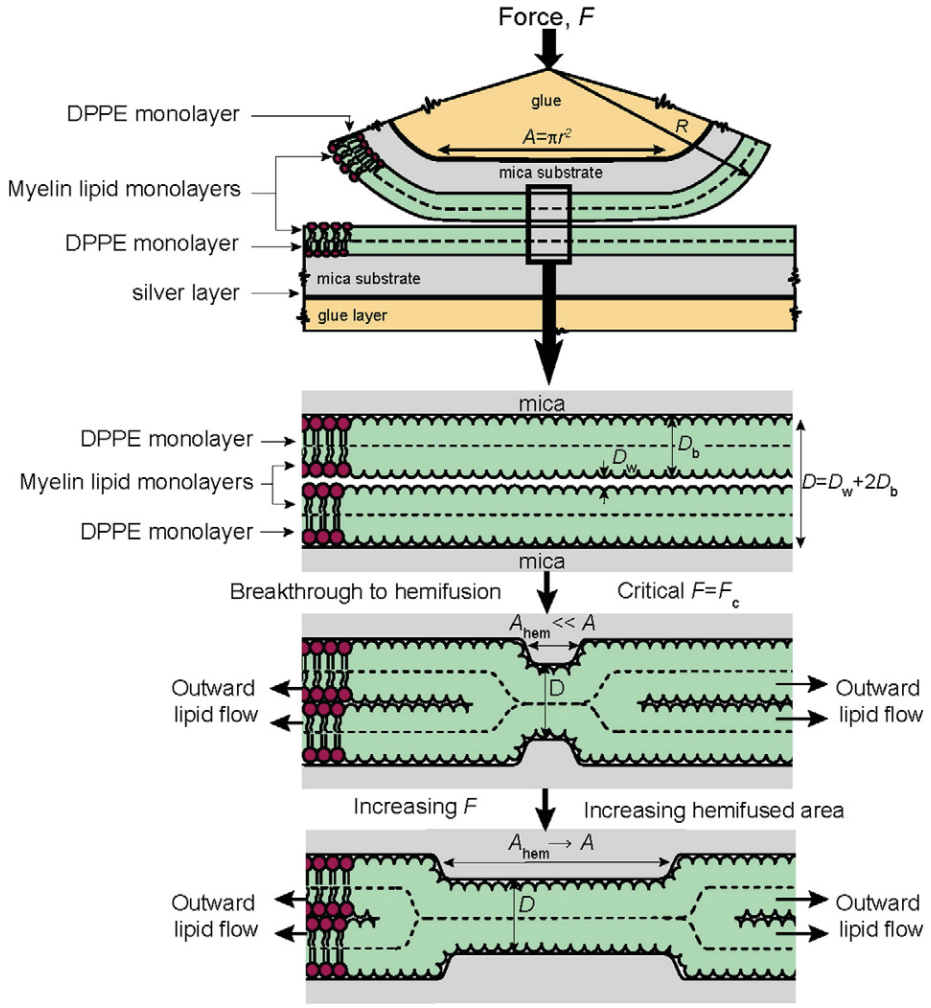

Fig. 1. Schematic representation of the hemifusion mechanism between two supported bilayers. Upon normal compression of the bilayers, the membranes undergo a sudden breakthrough that triggers the hemifusion event, which involves the outward flow of the outer monolayer lipids and expansion of the hemifused monolayer–monolayer contact over a period of ~5 min. The normal (or critical) force, F_c, at which this breakthrough occurs can be measured during the experiment as well as the hemifusion pore size using the FECO technique (see Materials and methods section for details).

interference fringes (also called fringes of equal chromatic order, FECO) using the equation [16]:

$$\tan(k\mu_w D)=\frac{2\overline{\mu}\sin(n\pi\lambda_n/\lambda)}{(1+\overline{\mu}^2)\cos(n\pi\lambda_n/\lambda)\pm(\overline{\mu}^2-1)} \quad (1)$$

where μ_w is, in a first approximation, the refractive index of water and $\overline{\mu}$ the ratio of the refractive indexes between mica and the solution between the mica surfaces (water). The distance resolution in our experiments was about 0.1–0.2 nm which depended mostly on the mica sheets thickness and optical alignment.

The normal interaction force function $F(D)$ between bilayers as a function of the mica–mica separation distance D was obtained by measuring the deflection of the double cantilever spring supporting the lower surface [17–19]. In particular, the local geometry of the contact zone, the shape of the interacting surfaces, the real contact area – with a normal resolution of 0.1–0.2 nm and a lateral resolution of 1 μm – can be extracted from the analysis of the FECO fringes [22]. Any localized defects, such as an initial sign of hemifusion, can be precisely visualized, quantitatively measured, and monitored using the FECO technique as a function of time and normal force (or pressure) [22,23].

3. Theoretical and experimental background

Previous studies [7,9] have developed different expressions for the total interaction energy W that included several components such as the electrostatic, "steric-hydration", van der Waals, and the undulation interaction. These models were developed to analyze experimental data obtained directly on myelin membranes ex-vivo using X-ray diffraction techniques such as the osmotic pressure technique [7,24]. Since our experimental geometry and setup is quite different, it is necessary to develop a model that adequately represents our experimental conditions of supported bilayers interacting in a reservoir rather than osmotically stressed membrane stacks. First, because we use lipid bilayers supported on a solid substrate in solution, the repulsive undulation forces are expected to be negligible. A more important difference of our setup is the very different elastic deformations of the bilayers upon normal compression. For example, in the osmotic pressure technique, water is osmotically sucked out from between the bilayers (a "dehydration" process) which causes the bilayers to *thicken* and the headgroup areas, a, to *decrease* as they come closer together [25–27]; and there are therefore no hemifusion or fusion events. In contrast, when two supported bilayers are locally pressed together in the SFA (i.e., surrounded by a reservoir of the solution) they locally *thin*, the exposed molecular area *increases*, more

hydrophobic groups (tails) become exposed, and local hemifusion events can now occur. Finally, our results clearly show that we also have to consider the contribution of the attractive hydrophobic force without which we could not model the observed hemifusion processes.

The final expression for the total interaction energy, W, was derived from the total *molecular* energy of the lipids in the bilayers, E, which can be written as [28]

$$E(D) = 2\gamma_i a_0 + \gamma_i \frac{(a-a_0)^2}{a} + C_{ES}e^{-D/D_{ES}} + C_{SI}e^{-D/D_{SI}} + C_{HI}e^{-D/D_{HI}} + \varepsilon\left(\frac{\sigma}{D}\right)^8 \text{ per molecule.} \quad (2)$$

where

$$W = E/a = F/2\pi R \text{ per unit area.} \quad (3)$$

The first two terms represent the total interfacial energy including the elastic energy per lipid molecule, a_0 being the optimal molecular area under no external stress, and γ_i the interfacial tension of the hydrocarbon–water interface [17]. The first exponential component stands for the electrostatic interaction, C_{ES} and D_{ES} being a constant pre-factor and the Debye length respectively. The second exponential component represents the steric-hydration interaction of characteristic decay length D_{SI} and pre-factor C_{SI} [29]. The third exponential component stands for the hydrophobic interaction which can be described by a single exponential term [30] with a characteristic decay length D_{HI} and a pre-factor C_{HI} accounting for the *excess* interfacial energy generated upon deformation of the bilayers which can be written as $C_{HI} = -\gamma_i(a-a_0)$ [31]. The last term of the equation is the simple Lennard–Jones potential acting at short separation distances between two planar surfaces. No van der Waals interaction term was added to E because this interaction has only a very small contribution in this system for separation distances less than $\sim 5D_{ES}$ given the low Hamaker constant of the system of approximately 6×10^{-21} J, and because the van der Waals interaction is also strongly screened due to the high salt content in the medium [17]. The molecular area of the lipid molecules, a, at any D can be explicitly obtained by considering that the lipid molecular volume is conserved during the bilayers' compression and deformation (thinning), given by $(dE/da) = 0$ at each separation distance, D.

The total equilibrium interaction energies $E(D)$ and $W(D) = E(D)/a$ between two flat surfaces and the interaction forces $F(D)$ of two cross-cylinder surfaces measured with the SFA can be related using the Derjaguin approximation at small separation distances: $W(D) = F(D)/2\pi R$. It is worth noting that, besides the fact that this model was developed to comply with our experimental conditions, it allows to capture many important aspects of lipid bilayer interactions that are not accessible using others techniques. For example, the AFM and/or the Osmotic Stress (OS) techniques cannot directly measure or observe fusion, can only measure repulsive forces (in the case of OS only), and cannot measure the interbilayer separation directly. Indeed, the model which includes both repulsive *and* adhesive interactions, as well as elastic deformations and hemifusion, cannot be currently tested quantitatively by any other technique.

The effective surface charge of the lipid bilayers can be calculated from the measured forces in the electrostatic interaction regime, given by [17]:

$$\frac{F(D)}{R} = \frac{Z}{D_{ES}}e^{-D/D_{ES}}, \quad (4)$$

where Z is an interaction constant defined by [32]:

$$Z = 64\pi\varepsilon\varepsilon_o\left(kT/e^2\right)\tanh^2(ze\Psi/4kT), \quad (5)$$

where ε and ε_o are the electric permittivity of the aqueous media and vacuum, respectively, k is the Boltzmann constant, T is the temperature, z is the valency ($z = 1$ for a monovalent electrolyte), e is the electronic charge, and Ψ is the surface potential of the membrane. The effective bilayer surface potential Ψ is related to the effective surface charge density, σ, by [32]:

$$\sigma = 0.117\sinh(\Psi/51.3)\text{C/m}^2 \quad (6)$$

at 24 °C where Ψ is in mV. By definition $\sigma = 1$ C/m^2 corresponds to one electronic charge per 0.16 nm^2 (16 Å^2).

4. Results

4.1. Hemifusion of model myelin lipid supported bilayers

Fig. 1 shows schematically a typical hemifusion process of two bilayers, which is characterized by a sudden breakthrough of the outer leaflets followed by an outward flow of lipids that allow the hemifused region to grow to its equilibrium size. Experimentally, bilayer hemifusion can be observed by analyzing the changing shapes of the FECO fringes ([23], Fig. 2). In most of the cases we studied, hemifusion occurred only when calcium was added to the buffer for both healthy and diseased membranes, and only occasionally in calcium-free buffer and only in the case of diseased membranes (see Fig. 2).

Analysis of the FECO fringes lead to the following observations: the hemifusion of diseased membranes always involves the formation of a pore and follows the mechanism described in Fig. 1. The hemifusion pore always nucleates in the central part of the contact circle, of area A, where the normal pressure is highest. Indeed, according to Hertz theory [33], the normal pressure at the center of the contact, P_{max}, is given by [22]:

$$P_{max} = \frac{3}{2}\frac{F}{A}, \quad (7)$$

where F/A is the average or mean contact pressure. The critical pressure, $P_c = (3/2)F_c/A$, at which the breakthrough typically appears was ~10 MPa. Once nucleated, the hemifusion pore of area A_{hem} expands until reaching the edges of the contact, as shown schematically in Fig. 1. The time from first nucleation to full hemifusion in equilibrium takes a few minutes, which is slower than previously observed for highly fluid bilayers, but faster than for bilayers in the gel state [21].

The origin of the breakthrough is an instability in the interaction force between the bilayers, as discussed in Ref. [31]. Initially, under increasing compressive load the bilayers deform elastically by thinning. Assuming constant lipid volume, the thinning of the bilayers leads to an increase of the molecular area of the lipids ($a > a_0$) which are accompanied by a lateral outward diffusion of the molecules. During the thinning of the bilayers, as a increases above a_0, the lipids expose hydrophobic regions (i.e., the hydrophobic tails of the lipids) that were not accessible under zero or low compression. The concomitant appearance of the hydrophobic interaction (see Eq. (2)) eventually leads to an instability in the interaction (a turning point in the energy) and causes hemifusion of the bilayers. Using Eq. (2), the onset of the instability was estimated to appear when the lipid molecular area, a, increased by approximately 25–30%, i.e., when a/a_0 reached ~1.25.

The hemifusion of *healthy* bilayers in the presence of calcium seems to follow a different mechanism. The FECO fringes analysis did not provide any evidence of a hemifusion pore (Fig. 2d). Rather, a fast thinning of the bilayers was observed leading eventually to monolayer–monolayer contact, as seen in the image sequence Fig. 2d–f. However, the onset of the thinning was estimated to also

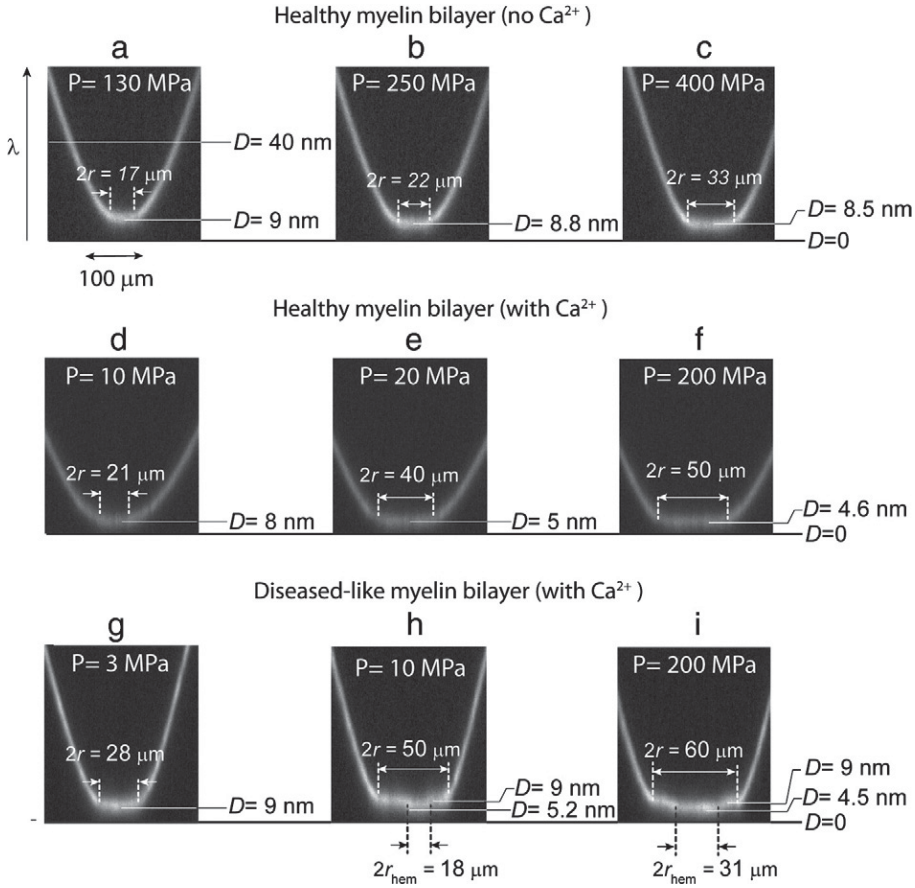

Fig. 2. Snapshots of the FECO fringes during normal compression of healthy and diseased myelin bilayers with and without calcium in the medium. In the healthy case (a–c), the contact deforms into a flat area that grows with the applied load without showing any evidence of strong adhesion, hemifusion or local deformation of the bilayers (a–c). After addition of calcium (d–f), healthy membranes thin significantly upon compression until reaching monolayer–monolayer contact. For the diseased bilayers (g–i), the applied compression triggers a local breakthrough at a pressure of $P_c \approx 10$ MPa that spreads throughout the contact area.

appear at a lipid molecular area approximately 30% higher than the non-stressed bilayers.

4.2. Interaction forces between myelin lipid bilayers

Force–distance, or energy–distance, measurements provide more insight into the hemifusion mechanism of bilayers at the molecular level. Fig. 3 shows the total interaction energy W measured between two flat diseased myelin bilayers as a function of the separation distance D (between the two mica substrates). The experimental data are fitted to the model given by Eq. (3), where curves for the total interaction energy as well as for the partial interaction energies are shown by solid lines. The effect of elastic deformation of the bilayers is seen as an inward shift of the repulsive electrostatic (ES) and steric-hydration (SI) interactions. Including the hydrophobic interaction (HI) captures the mechanical instability that triggers the onset of the hemifusion process. When separated from the fully hemifused state, i.e., from contact of the two DPPE monolayers at $D = D_{ad}$, the surfaces jump apart by a large distance indicative of a strong adhesion force.

The force–distance measurements shown in Fig. 4 highlight clear differences in the interaction forces between healthy (left) and diseased (right) myelin bilayers, as well as between calcium-free (green points and lines) and calcium containing solutions (red points and lines). When measured on approach, all the force–distance profiles show a repulsive exponential regime from large separations down to $D \approx 10$ nm, corresponding to bilayer–bilayer separation distances of $D_w \approx 1$ nm. This is the expected electrostatic double-layer interaction. The measured exponential decay length of $D_{ES} \sim 7$ Å is in agreement with the theoretical value for the Debye length of 7.8 Å. From Eqs. (4–6), the surface charge density of the bilayers was estimated to be $\sigma = 0.021$ C/m^2, or one electronic charge per 750 ± 150 Å^2, which corresponds to a degree of dissociation/ionization of the lipid headgroups of 65 ± 13%. This value is similar to, although somewhat higher than, values previously reported for both supported [21] and free bilayers [17,34]. Due to the large error associated to the measurements, we could not establish any differences in the surface charge densities between healthy and diseased myelin bilayers (both with and without calcium in the medium).

As the surfaces are pressed closer together from $D \approx 10$ nm to $D \approx 9$ nm, the steric-hydration repulsion and the elastic deformation (thinning) of the compressed bilayers take over as the dominating contributions to the repulsion. Fig. 4a and b shows that in calcium-free buffer (green points and curves) the repulsive steric-hydration forces and the membrane elasticity are strong enough to avoid hemifusion of *healthy* myelin bilayers, with only elastic compression occurring with *diseased* bilayers. The elastic moduli of the compressed bilayers can be extracted from the compression regimes (orange portions of the force profiles in Fig. 4a and b) as previously reported [35]. We obtained values of 67 MPa and 5.2 MPa for healthy and diseased bilayers, respectively. Thus, in calcium-free buffer, diseased lipid bilayers are in a more fluid state than healthy bilayers, more prone to elastic thinning, and (at least partial) hemifusion. This difference in fluidity is most likely due to the higher total fraction of unsaturated lipids (PC + PE + PS, see Table 1, second column) in the diseased bilayers.

As already mentioned, addition of 2 mM calcium leads to hemifusion of the bilayers for both healthy and diseased bilayers. As shown

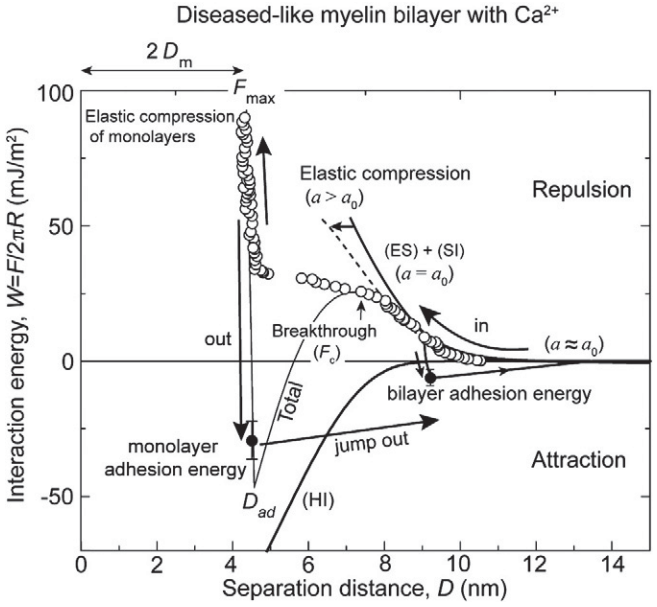

Fig. 3. Measured "force-law" F/R vs D (force–distance curves) and their representation in terms of the generic interaction model described by Eq. 2. The total interaction energy $W = F/2\pi R$ is plotted on the right, as well as its main components which include the attractive hydrophobic interaction (HI, thick solid line), the repulsive electrostatic interaction (ES) and the repulsive steric-hydration interaction (SI) which are connected via the elastic deformations of the bilayers as they are pressed together (Eq. (2)). The experimental data shown is for a diseased model bilayer compressed in 2 mM calcium buffer. The repulsive electro-steric component (ES + SI) of nondeforming bilayers is represented by a thick solid line. The dotted line represents the electrosteric interaction potential considering elastic deformation of the bilayers. Filled symbols represent adhesion energies measured by separating the surfaces until they jump out.

in Fig. 4 (red points and curves), the critical (normalized) forces for the onset of hemifusion occurred at $F_c/R = 75$ and 100 mN/m, corresponding to critical pressures of $P_c = 10$ and 13 MPa for healthy and diseased bilayers, respectively. Previous SFA experiments on model mixed lipid bilayers composed of uncharged (zwitterionic) and negatively charged lipids [21] have shown that calcium ions in the medium induce condensation of the negatively charged lipid headgroups, which promotes the formation of lipid domains in the bilayers. Here, too, the appearance of lipid domains upon calcium binding indirectly observed in the FECO fringes: at normal pressure close to the critical hemifusion pressure P_c the FECO fringes at the contact site appear rougher compared to those at lower applied pressures (larger separations). This roughness is due to local heterogeneities in the bilayers' thickness (optical path lengths) which was estimated at 0.1–0.3 nm, and which is the expected height difference between liquid ordered and liquid disordered bilayers (domains) [36]. It is possible, that these domains form once the bilayers (or outer monolayers) get close enough to each other, rather than already existing in the isolated (well-separated) bilayers [37].

As seen in Fig. 4c–d (red curves) in the presence of calcium the hemifusion processes of healthy and diseased myelin bilayers showed quite different behaviors. The pressure–distance profile of diseased bilayers (Fig. 4d) shows a single transition instability heralding the onset of the hemifusion, similar to the "van der Waals loop" in a P-V phase diagram that characterizes a two-phase coexistence regime. The measured maximum and minimum in the pressure–distance profile is due to the out-of-thermodynamic-equilibrium state of the bilayers during the compression, meaning that the experimental compression rate was too fast to allow the bilayers to reach their equilibrium (hemifused) state at $D = 2D_m$. The transition from the local maximum to the local minimum coincides with the final thinning and rupture of the bilayers.

The pressure–distance profiles measured with healthy myelin bilayers (Fig. 4c), show two van der Waals loops, each one representing a different transition state. In contrast to the breakthrough that was observed in diseased bilayers, the first loop/transition, occurring at $D = 9$ nm, probably corresponds to a thinning of the bilayers associated with a collective reordering of the (more ordered, less fluid) lipid molecules into a tilted configuration. The second transition appears to be the final squeeze out of the lipids from the contact area, leading to monolayer–monolayer contact in the fully hemifused state.

4.3. Time and load dependence of the adhesion forces between myelin lipid bilayers

Subtle changes in the lipid composition of myelin bilayers also had a profound impact on the calcium mediated adhesion both between the bilayers (separated without hemifusion) and monolayers (separated from the hemifused state). Divalent calcium ions Ca^{2+} are known to electrostatically bridge the headgroups of negatively charged lipids, both (laterally) within and (normally/trans) between bilayers [21]. No significant adhesion was measured between the bilayers in calcium-free buffer. The effects of calcium on the adhesion forces between fully developed (not fused) bilayers in the long-range interaction regime ($D > 2D_b$ in Fig. 4) were assessed by measuring the adhesion forces F_{ad}, corresponding adhesion energies W_{ad} and E_{ad}, and separation distances D_{ad} from where the surfaces jump out of contact on separating the bilayers. The contact times t_c were also measured since these were found to have a significant effect on the adhesion forces. The force profiles and adhesion forces on the very first approach and separation were not different from all subsequent approaches and separations so long as these were measured under the same loading conditions and contact times.

The results (Fig. 5) show how the adhesion energy, E_{ad} varied with the contact time t_c at a given applied load F_{max}. Below a certain load threshold, between 5 and 12 mN/m, corresponding to bilayer separations of $D_w > 1.5$ nm, no adhesive forces were measured for both healthy and diseased membranes independently of the contact time. Above these loads, or closer in, the adhesion forces (and corresponding energies) increased as $t_c^{1/2}$, which is characteristic of a diffusion process [31]. These results indicate: (1) that the bilayers have to come closer than a certain distance (of approximately $D_w < 1.5$ nm) for the (ionic) adhesion bonds to form, and (2) slow lateral diffusion occurs within the contact area as the negatively charged lipids and calcium ions find each other [21]. It is also noteworthy that small difference in lipid composition between healthy and diseased membranes results in a dramatic change of the adhesion: the healthy bilayers showed higher adhesion forces than the diseased bilayers (cf. Fig. 4a and b), an effect that became more pronounced for longer contact times.

5. Discussion and conclusions

Our studies of the effects of lipid composition on the adhesion and hemifusion of healthy and diseased model myelin bilayers show that the interaction forces (or energies) as a function of distance are well described by a generic model that includes the hydrophobic interaction between the bilayers in addition to the Derjaguin–Landeau–Verwey–Overbeek (DLVO) and steric-hydration interaction potentials commonly used to describe biological membranes. We showed that the consideration of the hydrophobic interaction in the model captures the instability that heralds the onset of hemifusion of the bilayers, highlighting the important role of the hydrophobic interaction in membrane adhesion and fusion processes in general.

Occurrence of hemifusion is expected to depend strongly on the phase state of the lipid bilayers, which itself depends on the lipid composition and chemistry. The size, shape and electric charge of each type of lipid as well as its interaction with cholesterol affects

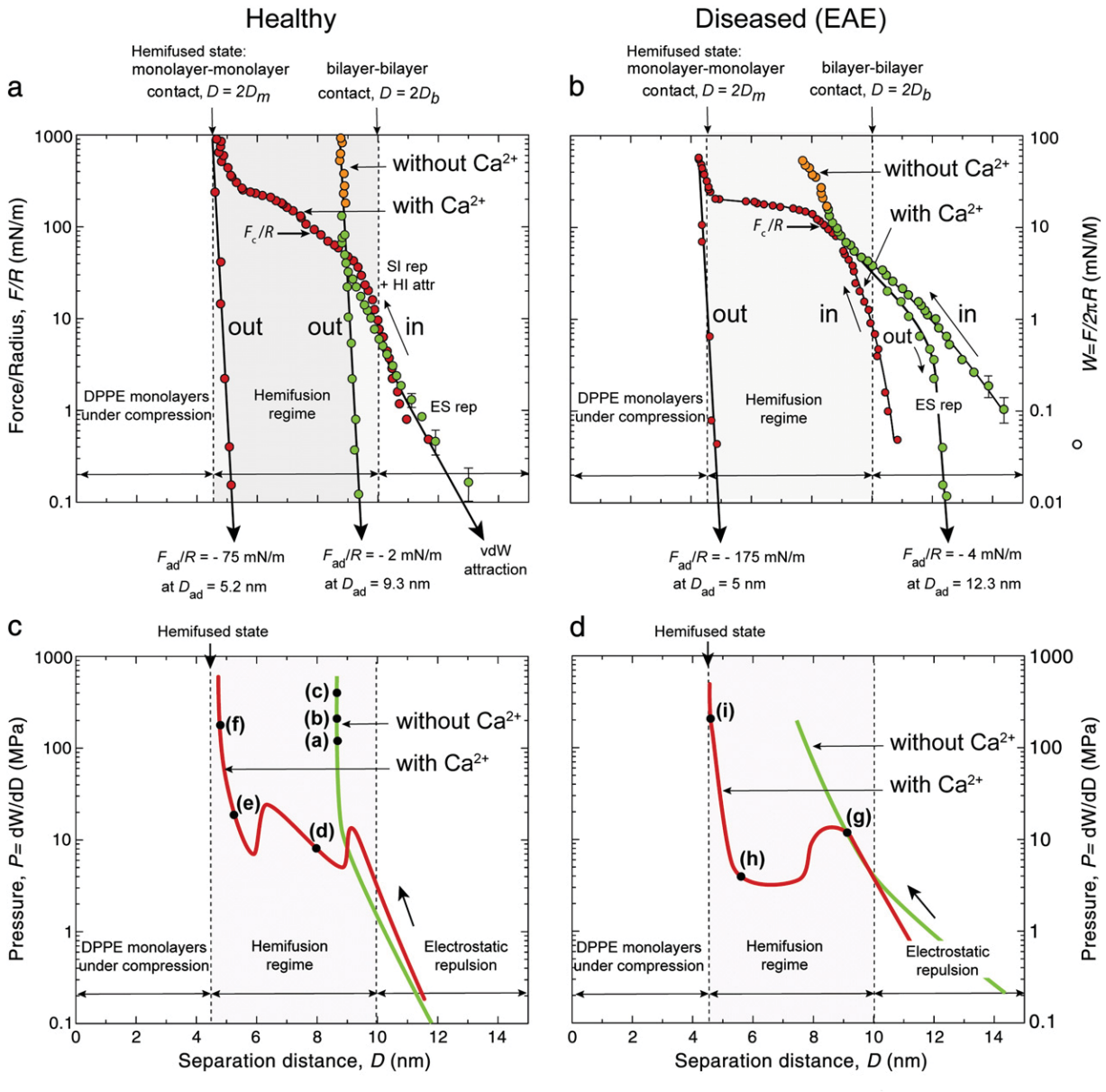

Fig. 4. Experimental force–distance (a and b) and pressure–distance (c and d) curves obtained from the SFA experiments for healthy (left) and diseased or EAE (right) model myelin lipid bilayers. In calcium-free buffer (green points and lines), healthy bilayers do not exhibit any signs of hemifusion while diseased membranes clearly show thinning and/or hemifusion (not shown). Addition of 2 mM calcium (red points and lines) promotes hemifusion in both model membranes, but the molecular mechanisms associated with hemifusion are quite different for the two types of bilayers, as discussed in the text. Labels **(a)** to **(i)** in panels c and d refers to the corresponding snapshots of the FECO fringes shown in Fig. 2. (For interpretation of the references to color in this figure legend, the reader is referred to the web version of this article.)

the fluidity of the bilayer. Bilayers with a high cholesterol content are in general in the liquid ordered state at room temperature, and they are known to hemifuse very slowly compared to fluid state bilayers [31] even under a large applied load. Our observation of a higher probability of the high cholesterol content diseased myelin bilayer to hemifuse and compress compared to the lower cholesterol content healthy bilayers is, in that respect, unexpected. However, diseased membranes exhibit smaller liquid ordered domains compared to healthy membranes, and at a higher density [1,38]. Domain boundaries are more likely to expose hydrophobic edges of the lipids which are a primary source of defects in bilayers that provide hydrophobic nucleating sites for hemifusion, thereby enhancing membrane fusogenicity.

In calcium-free solutions, healthy membranes did not hemifuse while diseased membranes hemifuse easily. Addition of 2 mM calcium favors the hemifusion of the bilayers independently of their composition, but the mechanisms involved were different for the healthy and diseased bilayers. In the case of diseased bilayers, calcium binding to and bridging of closely apposed bilayers results in the formation of domains that enhance bilayer–bilayer adhesion and lower the energy barrier to hemifusion. The hemifusion process was characterized by single transition which is similar to the "stalk model" [39]. In healthy membranes, no single breakthrough was observed during hemifusion; instead, two intermediate transition states were observed, most likely an initial transition to a tilted lipid state followed by the expulsion of the (tilted) lipids into the hemifused state. Bilayer–bilayer adhesive interactions were measured only in calcium solutions. The adhesion energy increased with the contact time as $t_c^{1/2}$, indicating a diffusion-controlled process for the formation of calcium bridges between the negatively charged lipid of apposing bilayers, similar to the kinetics previously observed for *hydrophobic* adhesion [31].

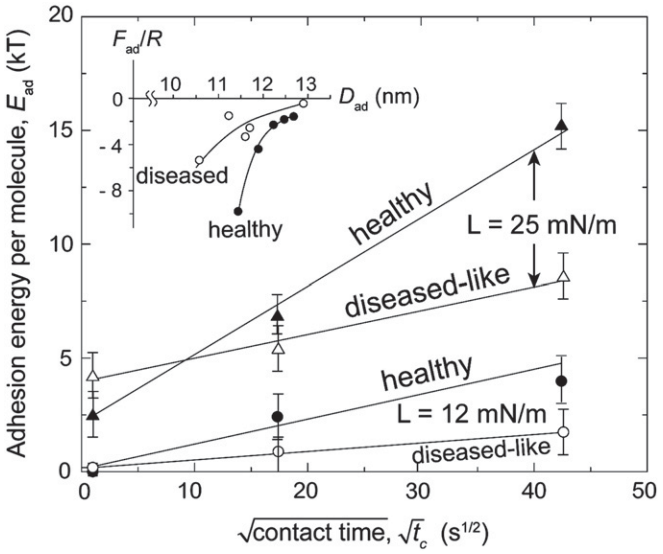

Fig. 5. Time evolution of the molecular adhesion energy under low applied maximum loads (12 and 25 mN), F_{max}. In these low load regimes, the adhesion between the bilayers is dominated by calcium ions bridges between the negatively charges lipids of the apposing membranes. The time evolution of the adhesion energy indicates that the bridging process is diffusion controlled (as previously observed for *hydrophobic* adhesion [31]). The differences observed between healthy and diseased membranes can be explained in terms of the lipid composition (see Results section for details). The inset shows the evolution of the adhesion force F_{ad}/R which gives the adhesion energies, E_{ad} and W_{ad}, as a function of the jump out distance D_{ad}.

Calcium is known to bind to a large variety of lipids, especially negatively charged lipids like PS. In terms of lipid content (without including cholesterol, see Table 1), both healthy and diseased membranes have a similar mole percent of PS, which indicates that the observed differences in adhesion energy must involve other lipids. Both PE and PC show 5–10% difference in mole content between healthy and diseased myelin bilayers, PE being present in higher content and PC in lower content in diseased bilayers. PE is known to have a higher affinity for calcium than PC [40]. The affinity of PE to calcium is known to also depend on other factors such as the pH and lipid packing/molecular area. Indeed, when the PE molecular area is less than 60 $Å^2$ its affinity for calcium decreases dramatically with lipid concentration. This effect has been explained [40] by the reduced accessibility of calcium to the phosphate group in closely packed lipid bilayers. Therefore, lipid membranes with a higher content of PE, i.e., more closely packed PE molecules, as in the case of diseased myelin membranes, are likely to exhibit a lower affinity for calcium binding and, therefore, lower ionic adhesion forces.

These results could be of particular relevance for understanding lesion development in MS. Indeed, most common lesions in MS are located in the myelin and involve changes in the supramolecular arrangement of the membranes. Among the most common defects observed in diseased myelin are: swelling of the myelin membranes due to a loss of inter-membrane adhesion, and vesiculation which is the result of multiple fusion or hemifusion events between the membranes.

Calcium concentration in myelin is known to fluctuate depending on numerous external factors and particularly under chemical ischemia [41]. Calcium ions have several deleterious effects on myelin membrane organization and structure. For example, calcium ions are known to catalyze myelin basic protein deimination by the Ca^{2+}-dependent peptidylarginine deiminase 2 which leads to a loss of adhesion between cytoplasmic lipid leaflets and MBP [42,43]. Calcium ions are also known to alter the fluidity of lipid domains and protein distribution like MBP. In particular, X-ray and SEM studies performed ex-vivo on myelinated axons have shown that aberrant concentrations of calcium can trigger swelling and vesiculation of myelin membrane involving dramatic changes in protein and lipid distribution [44,45].

Our study shows that lesion development could be the result of very minute changes of the composition of the lipid membranes and/or a variation in the calcium content of the cytoplasm, and the presence of domains (patches, or rafts) in the membranes. Our study shows that these three factors are related, and highlights the need to further investigate a possible relationship between the formation of lipid domains and the development of lesions in myelin and other membrane associated diseases.

Acknowledgements

This work was supported by the National Institutes of Health under grant number R01 GM076709.

References

[1] Y. Min, T.F. Alig, D.W. Lee, J.M. Boggs, J.N. Israelachvili, J.A. Zasadzinski, Critical and off-critical miscibility transitions in model extracellular and cytoplasmic myelin lipid monolayers, Biophys. J. 100 (2011) 1490–1498.
[2] Y. Min, K. Kristiansen, J.M. Boggs, C. Husted, J.A. Zasadzinski, J.N. Israelachvili, Interaction forces and adhesion of supported myelin lipid bilayers modulated by myelin basic protein, Proc. Natl. Acad. Sci. USA 106 (2009) 3154–3159.
[3] C.S. Raine, in: P. Morell (Ed.), Myelin, Plenum, New York, 1984, pp. 1–41.
[4] J.M. Boggs, M.A. Moscarello, Structural organization of human myelin membrane, Biochim. Biophys. Acta 515 (1978) 1–21.
[5] D.A. Hafler, Multiple sclerosis, J. Clin. Invest. 113 (2004) 788–794.
[6] M.G. Rumsby, Organization and structure in central-nerve myelin, Biochem. Soc. Trans. 6 (1978) 448–462.
[7] R.P. Rand, N.L. Fuller, L.J. Lis, Myelin swelling and measurement of forces between myelin membranes, Nature 279 (1979) 258–260.
[8] R.A. Ridsdale, D.R. Beniac, T.A. Tompkins, M.A. Moscarello, G. Harauz, Three-dimensional structure of myelin basic protein.2. Molecular modeling and considerations of predicted structures in multiple sclerosis, J. Biol. Chem. 272 (1997) 4269–4275.
[9] H. Inouye, D.A. Kirschner, Membrane interactions in nerve myelin.1. Determination of surface charge from effects of pH and ionic strength on period, Biophys. J. 53 (1988) 235–245.
[10] B. Ohler, K. Graf, R. Bragg, T. Lemons, R. Coe, C. Genain, J. Israelachvili, C. Husted, Role of lipid interactions in autoimmune demyelination, Biochim. Biophys. Acta 1688 (2004) 10–17.
[11] Y.F. Hu, I. Doudevski, D. Wood, M. Moscarello, C. Husted, C. Genain, J.A. Zasadzinski, J.N. Israelachvili, Synergistic interactions of lipids and myelin basic protein, Proc. Natl. Acad. Sci. USA 101 (2004) 13466–13471.
[12] C.A. Husted, D.S. Goodin, J.W. Hugg, A.A. Maudsley, J.S. Tsuruda, S.H. Debie, G. Fein, G.B. Matson, M.W. Weiner, Biochemical-alterations in multiple-sclerosis lesions and normal-appearing white-matter detected by in-vivo P-31 and H-1 spectroscopic imaging, Ann. Neurol. 36 (1994) 157–165.
[13] G. Saher, S. Quintes, K.-A. Nave, Cholesterol: a novel regulatory role in myelin formation, Neuroscientist 17 (2011) 79–93.
[14] J.N. Israelachvili, Y. Min, M. Akbulut, A.G. Alig, G. Carver, K. Kristiansen, E.E. Meyer, N.S. Pesika, K. Rosenberg, H. Zeng, Recent advances in the surface forces apparatus (SFA) technique, Rep. Prog. Phys. 73 (2010).
[15] E.T. Castellana, P.S. Cremer, Solid supported lipid bilayers: from biophysical studies to sensor design, Surf. Sci. Rep. 61 (2006) 429–444.
[16] J.N. Israelachvili, Thin-film studies using multiple-beam interferometry, J. Colloid Interface Sci. 44 (1973) 259–272.
[17] J.N. Israelachvili, Intermolecular & Surface Forces, Third ed. Elsevier Academic Press, San Diego, 2011.
[18] J.N. Israelachvili, G.E. Adams, Measurement of forces between 2 mica surfaces in aqueous electrolyte solutions in range 0–100 nm, J. Chem. Soc. 74 (1978) 975–1001.
[19] J. Marra, J. Israelachvili, Direct measurements of forces between phosphatidylcholine and phosphatidylethanolamine bilayers in aqueous-electrolyte solutions, Biochemistry 24 (1985) 4608–4618.
[20] N.W. Moore, T.L. Kuhl, Bimodal polymer mushrooms: compressive forces and specificity toward receptor surfaces, Langmuir 22 (2006) 8485–8491.
[21] D.E. Leckband, C.A. Helm, J. Israelachvili, Role of calcium in the adhesion and fusion of bilayers, Biochemistry 32 (1993) 1127–1140.
[22] R.G. Horn, J.N. Israelachvili, F. Pribac, Measurement of the deformation and adhesion of solids in contact, J. Colloid Interface Sci. 115 (1987) 480–492.
[23] C.A. Helm, J.N. Israelachvili, P.M. McGuiggan, Molecular mechanisms and forces involved in the adhesion and fusion of amphiphilic bilayers, Science 246 (1989) 919–922.
[24] D.A. Kirschner, Diffraction Studies of Myelin, in: P. Morell (Ed.), myelin, Plenum Press, New York, 1984, pp. 50–95.
[25] E.N. Serrallach, R. Dijkman, G.H. Dehaas, G.G. Shipley, Structure and thermotropic properties of 1,3-dipalmitoyl-glycero-2-phosphocholine, J. Mol. Biol. 170 (1983) 155–174.

[26] A. Tardieu, V. Luzzati, F.C. Reman, Structure and polymorphism of hydrocarbon chains of lipids — study of lecithin-water phases, J. Mol. Biol. 75 (1973) 711–733.
[27] Due to their interaction with lipids, stabilizing proteins may alter the thickening of the bilayers to a certain extent which depends on the protein-lipid interaction forces, free and interacting lipid distribution and protein content.
[28] S. Donaldson, B.F. Chmelka, J.N. Israelachvili, General hydrophobic interaction potential for surfactant/lipid bilayers from direct force measurements between light-modulated bilayers, Proc. Natl. Acad. Sci. USA 108 (2011) 15699–15704.
[29] R.P. Rand, V.A. Parsegian, Hydration forces between phospholipid bilayers, Biochim. Biophys. Acta 988 (1989) 351–376.
[30] E.E. Meyer, K.J. Rosenberg, J. Israelachvili, Recent progress in understanding hydrophobic interactions, Proc. Natl. Acad. Sci. USA 103 (2006) 15739–15746.
[31] C.A. Helm, J.N. Israelachvili, P.M. McGuiggan, Role of hydrophobic forces in bilayer adhesion and fusion, Biochemistry 31 (1992) 1794–1805.
[32] D. Leckband, J. Israelachvili, Intermolecular forces in biology, Q. Rev. Biophys. 34 (2001) 105–267.
[33] H.J. Hertz, Reine Angew. Math. 92 (1881) 156.
[34] A.C. Cowley, N.L. Fuller, R.P. Rand, V.A. Parsegian, Measurement of repulsive forces between charged phospholipid bilayers, Biochemistry 17 (1978) 3163–3168.
[35] Y.L. Chen, C.A. Helm, J.N. Israelachvili, Measurement of the elastic properties of surfactant and lipid monolayers, Langmuir 7 (1991) 2694–2699.
[36] A.J. Garcia-Saez, S. Chiantia, P. Schwille, Effect of line tension on the lateral organization of lipid membranes, J. Biol. Chem. 282 (2007).
[37] Y.S. Jho, R. Brewster, S.A. Safran, P.A. Pincus, Long-range interaction between heterogeneously charged membranes, Langmuir 27 (2011) 4439–4446.
[38] D. Lee, Y. Min, P. Dhar, A. Ramachandran, J. Israelachvili, J. Zasadzinski, Relating domain size distribution to line tension and molecular dipole density in model cytoplasmic myelin lipid monolayers, Proc. Natl. Acad. Sci. USA 108 (2011) 9425–9430.
[39] J. Zimmerberg, S.S. Vogel, L.V. Chernomordik, Mechanisms of membrane fusion, Annu. Rev. Biophys. Biomol. Struct. 22 (1993) 433–466.
[40] T. Seimiya, S. Ohki, Ionic structure of phopholipid membranes, and binding of calcium ions, Biochim. Biophys. Acta 298 (1973) 546–561.
[41] I. Micu, Q. Jiang, E. Coderre, A. Ridsdale, L. Zhang, J. Woulfe, X. Yin, B.D. Trapp, J.E. McRory, R. Rehak, G.W. Zamponi, W. Wang, P.K. Stys, NMDA receptors mediate calcium accumulation in myelin during chemical ischaemia, Nature 439 (2006) 988–992.
[42] A.A. Musse, Z. Li, C.A. Ackerley, D. Bienzle, H. Lei, R. Poma, G. Harauz, M.A. Moscarello, F.G. Mastronardi, Peptidylarginine deiminase 2 (PAD2) overexpression in transgenic mice leads to myelin loss in the central nervous system, Dis. Model. Mech. 1 (2008) 229–240.
[43] A.A. Musse, E. Polverini, R. Raijmakers, G. Harauz, Kinetics of human peptidylarginine deiminase 2 (hPAD2) — reduction of Ca(2+) dependence by phospholipids and assessment of proposed inhibition by paclitaxel side chains, Biochem. Cell Biol. 86 (2008) 437–447.
[44] V. Melchior, C. Benitez, D.L.D. Caspar, Calcium and tetracaine induce close-stacking of myelin membranes by flocculation of lipid bilayers, Biophys. J. 21 (1978) 37A.
[45] V. Melchior, C.J. Hollingshead, D.L.D. Caspar, Divalent-cations cooperatively stabilize close membrane contacts in myelin, Biochim. Biophys. Acta 554 (1979) 204–226.